



## SWEET Call 1-2020: DeCarbCH

### Deliverable report

<b>Deliverable n°</b>	1.2.2
<b>Deliverable name</b>	Model documentation for thermal-ESM
<b>Authors</b> The authors bear the entire responsibility for the content of this report and for the conclusions drawn therefrom.	Jonathan, Chambers, UNIGE, Jonathan.chambers@unige.ch
<b>Delivery date</b>	3 2024

### Table of contents

<b>Summary</b> .....	<b>3</b>
<b>1 Introduction</b> .....	<b>4</b>
<b>2 Deliverable content</b> .....	<b>4</b>
2.1 Climate Data .....	4
2.2 Building Data .....	4
2.3 Building Heat Demand .....	4
2.4 Building Cooling demand .....	5
2.4.1 Modelling method for cooling demand in the service sector.....	5
2.4.2 Forecasting future space cooling demand.....	6
2.5 Thermal Network .....	7
2.5.1 Road network topology and routing .....	7
2.5.2 Multi-level Clustering.....	7
2.5.3 Flow analysis.....	7
2.5.4 Associating networks with thermal resources .....	8
2.5.5 Pump modelling.....	8
2.5.6 Fifth Generation district heating and cooling (5GDHC).....	8
2.6 Techno-economic parametrization of technology options.....	8
2.6.1 Retrofits .....	9
2.6.2 Heat pumps.....	9
2.6.3 Thermal networks .....	9
2.7 Application of the models in sensitivity analysis .....	9
2.7.1 Sensitivity analysis of fifth generation district heating and cooling coupled with borehole thermal energy storage with respect to cooling adoption .....	9



	2.7.2 Hydraulic Modeling of Thermal Grid Systems for Minimizing Pumping Energy Consumption.....	12
<b>3</b>	<b>Conclusion.....</b>	<b>14</b>
<b>4</b>	<b>References.....</b>	<b>14</b>



## Summary

The deliverable 1.2.2 consists of a model that integrates several research outputs from the SWEET DecarbCH project for thermal energy system modelling at the city and district scale. It consists of a set of modules with model components for heat demand, network routing, and climate data. The heat demand model uses building archetypes based on age, size, and destination of use to map typical energy demands and load curves shapes drawn from measured data to specific buildings in the input dataset. For heat demand in future use, an algorithm is used to evaluate the renovation potential of buildings and the techno-economic potential energy demand reduction. The model data includes a raster aggregate summary of building stock characteristics and heating demand models, as well as a dataset for building physical parameters. The building heat demand dataset includes fields for building footprint area, total estimated area, residential area, non-residential area, energy reference area, energy reference area of main residences, and the number of buildings of a given type.



## 1 Introduction

Deliverable 1.2.2 complements 1.2.1 with additional documentation for the model. As stated in D1.2.1, key references for model include an overview [1], heat demand model [2], building renovation model [3], and network layout algorithm [4]. These references provide additional detail and documentation. This section references the thermal energy system modelling at the “mesoscale”, e.g. city and district scale.

## 2 Deliverable content

The model consists of a package integrating modules components for heat demand, the network routing described above, and climate data. These modules are documented in the following sections.

### 2.1 Climate Data

The model's climate data consists of TMY data from <https://climate.onebuilding.org> delivered in an EnergyPlus Weatherfile (.epw) format. TMYx datasets are created as typical meteorological data derived from hourly weather data from 2021 in the ISD (US NOAA's Integrated Surface Database) using the TMY/ISO 15927-4:2005 methodologies. Future climate data is derived from the CMIP6-collection Swiss Regional Climate Model [5].

### 2.2 Building Data

The Swiss buildings registry (RegBL) is the primary source of building data. However, this dataset is known to be incomplete and contain some errors. It is assembled from data collected by Swiss cantons, which can introduce data harmonisation issues. Furthermore, only residential buildings are required by law to be present in detail in the registry. Most Cantons include data on other building types but some errors may appear as a result. For example, in some cases only the residential part of a mixed residential and non-residential building was recorded as the building floor area in the database. We therefore introduce heuristics to complete and correct the RegBL with other Swiss national open access datasets, notably the Swisstopo swissTLM3D [6] in order to ensure that building areas are consistent. Floor areas are particularly important [7], and were calculated using residence areas and building footprints and numbers of floors. Missing values were filled using the Swiss building geometry dataset. Energy Reference Areas (ERA), being the building areas that are thermally conditioned, were also calculated, and account for features such as stairwells and storage areas, etc. For residential buildings, statistical work was used to assess the relation between total area and heated area [7]. For non-residential buildings (especially service sector buildings), the ERA is the total floor area. Datasets corresponding were archived in the “frictionless data package” format [8]. This dataset summarises the characteristics of Swiss building stock on a raster basis at a resolution of 200x200m. Buildings from the Swiss building registry are categorised into 63 archetypes according to their age, use, and location following the work in [9], [10], [11], [12]. The location from the original work was converted into pixel coordinates. Only pixels containing at least one building were stored, resulting in 189315 pixels and 695488 points with unique pixel, age, and building type. Parameters for each archetype per pixel were calculated. This data was collated from multiple sources, starting with the Swiss building registry [13]. The dataset has 7 fields for 63 archetypes, although most pixels include only a subset of archetypes, resulting in 4 868 416 data points in total. <https://doi.org/10.26037/yareta:sluzlbggmjfxjj7qmyptxs7zoa>.

### 2.3 Building Heat Demand

For heat demand load, an algorithm for generating load curves according to the annual heating and hot water demands was based on measured climate-corrected load curves for all points of the territory. The current algorithm is adapted from the work in [2] and [16]. Briefly, the model uses building archetypes based on age, size, and destination of use to map typical energy demands and load curves shapes drawn from measured data to specific buildings in the input dataset. The yearly demands are based on climate corrected energy demand per m<sup>2</sup> for building archetypes defined by building type (single family, multifamily, office, etc.) and construction year. Energy demand intensities are mainly based on measured data. For heating and domestic hot water, the model calculates: yearly useful energy demand, yearly final energy demand, heating system efficiency, heating system fuel co<sub>2</sub> emissions intensity,



yearly co2 emissions, hourly load curves. Power loads are summarised as the 25th, 50th, 75th, 95th, 99th, percentiles and the maximum for useful and final energy, and 23 data fields were produced (15996224 points).

A second heat demand estimate uses the 'SwissRes' method (an archetype model derived from the building energy efficiency labelling database) [9], [10], [11], [12]. This model estimates potential energy savings if the building archetypes were renovated to high energy efficiency standards (Minergie label equivalent). Data from [17] was mapped onto the pixel grid (6 data fields, 4'172'928 data points).

Heat demands for the future use employ an algorithm to evaluate the renovation potential of buildings [14]. The techno-economic potential energy demand reduction has been evaluated in [3]. The method used in this work was implemented as a series of scripts and continued development conducted in [15]. These scripts can be obtained with open access.

## 2.4 Building Cooling demand

A Monte Carlo model of service sector building cooling demand is used for the service sector buildings [18]. This considers both current demand and projections of future demand based on climate and adoption rates. Cooling demand in service sector buildings—offices, hotels, retail, and health related buildings—was estimated for the present day and under different future climate change scenarios for Switzerland [19], [20]. Cooling energy demand curves are used from the PACE dataset derived from the Mangoret model. This provides simulated cooling demand curves for archetypical buildings (simulations performed with EnergyPlus) [21].

### 2.4.1 Modelling method for cooling demand in the service sector

The method for cooling demand in the service sector is reproduced here on the basis of published works [19], [20]. To estimate the space cooling demand of each service sector building, the following data characterising the space cooling equipment is required: presence of space cooling equipment (whether the building is being actively cooled), cooled floor area, cooling power intensity (defined in terms of cooled floor area), operating hours (equivalent full-load hours), and Coefficient of Performance (COP). The cooling characteristics data provided by Geneva cooling system permits covers a small portion of the Swiss service building stock, while comprehensive data on building characteristics (e.g. number of floors and service area) are available in RegBL. Therefore, a Monte Carlo simulation is applied to randomly assign cooling characteristics from approximated probability distributions, which are regressed on building characteristics. The model is separately applied to offices, trade, hotels, and health-related services.

#### 2.4.1.1 Define the probability distributions of cooling characteristics

Statistical analyses of empirical cooling data are performed to define probability distributions for each cooling characteristic. In cases where a dependence of a cooling characteristic on building characteristics is identified, the dependence is implemented in the probability distribution. To prepare the data from which the probability distributions are derived, the RegBL building data for the Canton of Geneva is combined with the Geneva cooling system permits data using the unique building identifier (EGID).

As cooling permits are compulsory in Geneva, we may assume that all buildings in Geneva for which a cooling permit exists have space cooling equipment installed, while those without a permit have no space cooling. This allows us to define a variable for the presence or absence of space cooling. The presence of space cooling equipment  $\delta$  is modelled as a Bernoulli distribution. The probability of the presence of space cooling equipment  $Pr$  is assumed to depend on building characteristics. The logistic regression model is fitted based on the service building stock in Geneva. Building characteristics selected as possible predictor variables are building age, log10 of ground area ( $\log_{10} A_{ground}$ ), number of floors, log10 of total area ( $\log_{10} A_{total}$ ), and log10 of service area ( $\log_{10} A_{service}$ ). Building age is a 6-category variable and is converted to 5 dummy variables.



For the remaining parameters, we only use data for buildings which have space cooling. We have both the service area from the RegBL and the cooled floor area from the cooling permits. This implies that when a building has space cooling, it is not the entire service area that is actively cooled. The cooled floor area is assumed to be proportional to the service area of the building. The relation between cooling power intensity and cooled floor area is modelled by a log-linear model. Parameters are estimated by applying a linear regression with logarithmic transformations [22]. The logarithmic transformation of cooling power intensity is found to be optimal according to the Box-Cox Test [23]. The transformation on cooled floor area is selected via AIC among several commonly used transformations: no transformation, square root, logarithm, and reciprocal.

A noise term is added to the cooling power intensity to model the unidentified diversity among buildings, i.e. thermal insulation level, occupant behaviours, etc. The number of operating hours NH is sampled from the empirical distribution of values recorded in the cooling permits. The cooling system's COP is also sampled from the empirical distribution of COP of the cooling systems present in the cooling permits. No correlation was found between NH or COP and other building characteristics.

#### **2.4.1.2** Generate cooling characteristics randomly from probability distributions

Before generating cooling characteristics for all buildings in the service sector, missing building characteristics are filled by randomly sampling from existing values, such as service area and number of floors. For each building, the presence of space cooling equipment is first assigned by randomly sampling from the Bernoulli distribution, which takes the value 1 (presence) with the probability of presence  $Pr$  predicted by the logistic regression model. Then, only for buildings predicted to have  $\delta$  values equal to 1 (i.e. presence of space cooling equipment), the characteristics required for calculating space cooling demand, such as cooled floor area, cooling power intensity, operating hours, and COP, are generated from the probability distributions defined in step 1).

The variation of climate among cantons is also integrated into the model. Since we have cooling data only for the canton of Geneva, the probabilities of presence of space cooling equipment is scaled according to the local historical maximum CDD. And the cooling energy intensity (product of cooling power intensity  $p_{cooling}$  and number of operating hours  $NH$ ) is scaled according to local CDD.

#### **2.4.1.3** Aggregate the results of space cooling demand

To estimate the space cooling demand of the service sector, building specific cooling demand is aggregated first for each subsector and second for the entire service sector. Parameter aggregates are calculated: total service area equals sum of  $A_{service}$ ; total cooled floor area equals sum of  $A_{cooled}$ ; saturation rate SR equals total cooled area divided by total service area; total space cooling demand equals sum of  $Q_{cooling}$ ; average cooling energy intensity  $q_{cooling,avg}$  equals total space cooling demand divided by total cooled floor area; total electricity demand for cooling equals sum of  $E_{cooling}$ ; average electricity intensity for cooling  $e_{cooling,avg}$  equals total electricity demand for cooling divided by total cooled floor area; and average coefficient of performance  $COP_{avg}$  equals total electricity demand for cooling divided by total space cooling demand. In accordance with the Monte Carlo method, steps are repeated for sufficient iterations to generate stable distributions of the aggregated sector level parameters. The mean and confidence interval are estimated.

### **2.4.2** Forecasting future space cooling demand

#### **2.4.2.1** Climate change

To evaluate the impact of climate change on cooling demand, we estimate future cooling demand under three climate scenarios: RCP 2.6, RCP 4.5, and RCP 8.5. CDDs are calculated based on Equation 1, using a 2km grid climate simulation ensemble dataset, allocated to buildings in the service sector by mapping the building location. Building specific cooling demand is calculated according to future CDD scenarios [24].



#### 2.4.2.2 Diffusion of space cooling equipment

At the building level, the diffusion of space cooling equipment is reflected in the probability of presence of space cooling equipment and potentially cooled floor area ratio. We assume the cooled floor area ratio will remain the same in the future, since stable average cooled floor area ratio was observed over the years in the input data. Therefore, in this study, we only consider the impact of the changing probability of the presence of space cooling equipment. This is modelled by the linear fit between the share of cooled buildings and the historical maximum CDD observed in the Genevan permit data, following the work of Bird et al. [25]. Genevan permit data is used despite the small sample size because the data from literature is not readily usable by a study with this different a scope [26], [27], [28]. Further data collection is required to investigate the impact of climate change on the diffusion of space cooling.

The probabilities predicted by the logistic regression are scaled for each year up to the scenario time horizon (2050). The scaling is calculated using the maximum CDD (derived from the future climate scenarios) experienced in the period up to and including the scenario year.

Temperature projections for 2050 under representative concentration pathways (RCP) RCP2.6, RCP4.5, RCP8.5 were used in addition to a reference scenario for the year 2015. By using a Monte Carlo simulation, the means and standard deviations for cooling demand in the different scenarios were calculated. Because of the lower number of buildings in the service sector, results were aggregated at a lower 400x400m resolution for each service building category, giving 6778 pixels, 33890 points with unique pixel and sector for each climate scenario. Cooling demand in the service sector: <https://doi.org/10.26037/yareta:5pdsn2n5yzesjn6xjda4w7keby> .

### 2.5 Thermal Network

An algorithm is used for calculating the optimised District Heat Network (DHN) layout, based on the road layout and the spatial distribution of demand and production points. This is based on a method published in [4] and reproduced below.

#### 2.5.1 Road network topology and routing

To calculate routing distances for a network connecting buildings, we must define a road network topology and routing distances between buildings through the road network. The spatial connectivity (i.e. nearest neighbourhood) of buildings was modelled as a graph defined by the Delaunay triangulation of building locations. For each edge in the Delaunay graph, we calculate the distance through the road network using Dijkstra's algorithm and store this as an edge weight in the graph. To calculate the total distance between an arbitrary pair of buildings, we calculate the shortest path through the Delaunay graph using the pre-calculated distance weights. For each row in the Delaunay edge table, the weight field was assigned.

#### 2.5.2 Multi-level Clustering

We observe that buildings are very unevenly spatially distributed into dense clusters and that network analysis only requires buildings that are close by. For each cluster generated by the top-level clustering, we apply processing and filtering followed by a second stage of clustering, making this a 'multi-level' clustering approach. To perform spatial clustering, DBSCAN was applied as it is a well-established algorithm suitable for geospatial applications where clusters are of varying density and non-convex [40] [41]. The Euclidean distance is used as the distance metric between points. The road distance between every building pair in a cluster is pre-calculated. The shortest distance via roads for every pair of buildings in a cluster is calculated using Dijkstra's algorithm subject to the road distance edge weights in the Delaunay triangulation mesh.

#### 2.5.3 Flow analysis

To estimate the thermal flow through the MST graph for the sub-cluster of size M a simplifying approximation is made that all flows travel from a given graph node (building) out to each building.



Therefore, flows through any graph edge are the sum of the flow to the graph node (building) at the end of the edge and any further downstream nodes. The flow to a given node in this case is set by the heat demand of the building, which is part of the building data table.

#### 2.5.4 Associating networks with thermal resources

To connect networks with resources like Borehole Heat Exchange (BHE), the method developed within the DecarbCH project and published in [42] is applied. This method optimises allocation of energy resources within a graph of spatially connected locations, accounting for constraints on the connection between resource and demands. A specific module was developed for using shallow geothermal energy in this context [43]. The layout of the network is designed by the geospatial network routing method developed by Chambers [44].

#### 2.5.5 Pump modelling

Basic modelling of hydraulic energy losses in the network is performed by summing the head losses from pipe friction and heat exchangers. Friction losses are estimated using the required mass flow rates and the Darcy-Weisbach equation that is solved in its implicit form. Heat exchanger head losses are taken from specification sheets.

#### 2.5.6 Fifth Generation district heating and cooling (5GDHC)

A model for the design and operation of the 5GDHC system supplied by BTES is presented in this section, reproduced from [45]. The model sizes the three major components and simulates their operation: building substations equipped with BHPs, a 2-pipe thermal network, and BHEs. The model considers a time horizon of one year, with a time step  $\Delta t$  of one hour.

##### 2.5.6.1 System design

###### 2.5.6.1.1 *Building substations*

A building substation connects the building's energy system with the thermal network. It is equipped with a BHP to supply  $\dot{Q}_h$ , and HX to supply  $\dot{Q}_c$ . Water circulation pumps (WCP) are used to control the mass flow rate passing through the substation.

###### 2.5.6.2 Generation units

The residual demand of a thermal network is supplied by a Borehole Thermal Energy Storage (BTES) made up of BHE fields when total substation loads do not counterbalance each other. It serves as a seasonal storage, enabling balancing of heating and cooling demands that occur in different periods over the year. If the local available area to install a BHE is insufficient to meet all demands, supplementary generation units are added. In this model, the default choice is a central biogas boiler and a central chiller, as they are widely available. Other energy conversion technologies could also be considered when required.

###### 2.5.6.3 Operation simulation of 5GDHC

In the operation simulation process, it is essential to evaluate the energy balance and hydraulic balance in the 5GDHC using the COP of the BHP calculated based on fluid temperature in the thermal network. Since the fluid temperature, mass flow rate, and heat transfer in boreholes are dependent on each other, an iterative process is required [46], [47].

## 2.6 Techno-economic parametrization of technology options

This section defines the models for the cost and energy use for the technologies considered: retrofits, decentralised heat pumps, and low- and high- temperature thermal networks fed in both cases by large (centralised) heat pumps. For each technology T we define the terms for technology investment  $I_T$ , operation and maintenance costs  $OM_T$ , and energy supply (or fuel) costs  $CE_T$ . These parametrisations are reproduced in large part from the work published in [48].



### 2.6.1 Retrofits

Retrofit investment costs and associated energy savings are derived from work by Streicher et al. [23,37], who define a cost for the deep retrofit (up to the Passivhaus standard) for building archetypes, which represent typical building types in Switzerland. These are determined for each building from a combination of the location, age, and current heating system.

### 2.6.2 Heat pumps

The cost per kW for a heat pump is a function derived empirically as a function of the archetype peak power per building  $P_{max,A}^{\square}$  of the form  $\alpha * P_{max,A}^{\beta}$ . This function approaches infinity for small P and zero for large P, and therefore the input values of  $P_{max}^{\square}$  are clipped to the range of input data from which the  $\alpha$  and  $\beta$  parameters are derived.

### 2.6.3 Thermal networks

Calculation of the thermal network application and cost is based on algorithms developed in [38]. The different DHN technologies have different constraints with respect to the building heat demand intensity ( $kWh.m^{-2}$ ) where they can be applied. Therefore, the subset of archetypes where the DHN is applicable is determined by applying constraints on the specific heat demand per building archetype, keeping archetype data where  $q_{min,T} < q_A < q_{max,T}$ .

## 2.7 **Application of the models in sensitivity analysis**

An important benefit from the development of the model package and programming API is the simplification of further analysis and automated research workflows. This is particularly the case for sensitivity analysis, which requires running large numbers of model iterations with parameter variations. Such an approach would not be possible if each component of the overall model resided in a different package or even a different software entirely (e.g. if a separate software needs to be used for doing the network simulation).

Two examples of application in sensitivity analysis are provided below. The first; “Sensitivity analysis of fifth generation district heating and cooling coupled with borehole thermal energy storage with respect to cooling adoption” is reproduced in part from a work presented at the CISBAT2023 conference [49]. The second; “Hydraulic Modelling of Thermal Grid Systems for Minimizing Pumping Energy Consumption” presents ongoing work presented in poster format at the DecarbCH Networking Conference 2024.

### 2.7.1 Sensitivity analysis of fifth generation district heating and cooling coupled with borehole thermal energy storage with respect to cooling adoption

This work was conducted to better understand the model behaviour of the previously published results on the potential of fifth generation district heating and cooling [49].5GDHC is a promising solution for decarbonising building thermal demands, as it allows for simultaneous heating and cooling through a bi-directional network. To assess the level of uncertainty in the key performance indicators (KPI) of 5GDHC, a Monte Carlo (MC) simulation [50] is conducted. Twenty parameters are investigated, which include building energy demand, final energy price and emission factor, equipment costs, and equipment efficiencies. The probability distributions of these parameters are summarized in Table 1. Sobol low discrepancy sequences are used to generate 2048 samples of each uncertain parameter, which were then fed into the 5GDHC model to obtain the KPIs of 5GDHC and the reference systems.

Table . Probability distribution of input parameters.

Uncertain parameter	Symbol	Probability distribution
Retrofit probability (yes/no, by building)	$p_{ret}$	$U(0,1)$
Carnot effectiveness <sup>1</sup> of BHP	$\eta_{CE,BHP}$	$0.5 * N(1,0.2)$
Carnot effectiveness of ASHP	$\eta_{CE,ASHP}$	$0.4 * N(1,0.2)$
Efficiency of gas boiler	$\eta_{boiler}$	$0.9 * N(1,0.2)$
Price of electricity [CHF/kWh]	$P_{elec}$	$0.283 * U(0.5,1.5)$



Price of gas [CHF/kWh]	$P_{gas}$	$0.120 * U(0.5,1.5)$
Emission factor of electricity [kg CO <sub>2</sub> /kWh]	$EM_{elec}$	$0.125 * U(0.5,1.5)$
Unit price of BHP [CHF/kW]	$P_{BHP}$	$1200 * N(1,0.2)$
Unit price of BHE [CHF/BHE]	$P_{BHE}$	$18500 * N(1,0.2)$
Scale factor of pipe cost	$SF_{pipe}$	$N(1,0.2)$
Price of ASHP [CHF/kW]	$P_{ASHP}$	$2000 * N(1,0.2)$
Price of chiller [CHF/kW]	$P_{chiller}$	$2000 * N(1,0.2)$
Price of gas boiler [CHF/kW]	$P_{boiler}$	$470 * N(1,0.2)$
O&M <sup>2</sup> factor of BHP [%]	$OM_{BHP}$	$2.5 * N(1,0.2)$
O&M factor of BHE [%]	$OM_{BHE}$	$0.5 * N(1,0.2)$
O&M factor of pipe [%]	$OM_{pipe}$	$1.0 * N(1,0.2)$
O&M factor of ASHP [%]	$OM_{ASHP}$	$3.5 * N(1,0.2)$
O&M factor of chiller [%]	$OM_{chiller}$	$2.5 * N(1,0.2)$
O&M factor of gas boiler [%]	$OM_{boiler}$	$3.0 * N(1,0.2)$
Discount rate [%]	$r$	$U(0,5)$

<sup>1</sup>Equals the efficiency of BHP divided by the Carnot efficiency.

<sup>2</sup>Operation and maintenance.

### 2.7.1.1 Global sensitivity analysis

We focus on identifying the most important sources of uncertainty in the upfront cost and levelized cost of energy of 5GDHC, since they are the main barriers for 5GDHC adoption. Sobol analysis [51], a variance-based global sensitivity analysis technique, is used to decompose the variance of model output into contributions from uncertain parameters and their interactions. We calculate the first-order Sobol indices, which quantify the effect of each parameter alone, and total-order Sobol indices, which measure the variance caused by each parameter, including its interactions with other parameters. This approach requires 22 000 MC runs.

### 2.7.1.2 Factor mapping

The objective of factor mapping is to determine the parameters responsible for 5GDHC's superior economic performance compared to the reference systems. Monte Carlo Filtering (MCF) [52] was performed by following these steps: 1) we define a criterion as '5GDHC has a lower levelized cost of energy than the alternative'; 2) we divide all MC runs into two subsets based on this criterion; 3) we conduct two-sample Kolmogorov-Smirnov (K-S) [53] tests to compare the probability distributions of each parameter in the two subsets.

### 2.7.1.3 Results

#### 2.7.1.3.1 Variation in 5GDHC performance

Figure 2 illustrates the variation in KPIs of 5GDHC and the reference systems. The levelized cost of supplied thermal energy (useful energy) of 5GDHC ranges from 170 to 430 CHF/MWh (5<sup>th</sup> and 95<sup>th</sup> percentiles), with approximately half of the MC runs indicating a smaller levelized cost of energy than the Electrification option, while only one-third of the cases indicate that 5GDHC outperforms the Business as Usual (BAU) option. The upfront cost of 5GDHC ranges from 150 to 610 million CHF, which is substantially larger than the reference systems. BHE (which constitutes BTES) and BHP contribute the most. In contrast, 5GDHC show better results in terms of environmental and technical performance. In the majority of MC runs, 5GDHC results in lower emissions and less energy consumption than the reference systems. This can be attributed to the higher efficiency of heat pumps when connected to a low-temperature heat source from BTES compared to air source heat pumps in the Electrification option and compared to gas boilers in BAU. Although the BAU option typically has the lowest electricity peak load, 5GDHC generally reduces the electricity peak load when compared with the Electrification option.

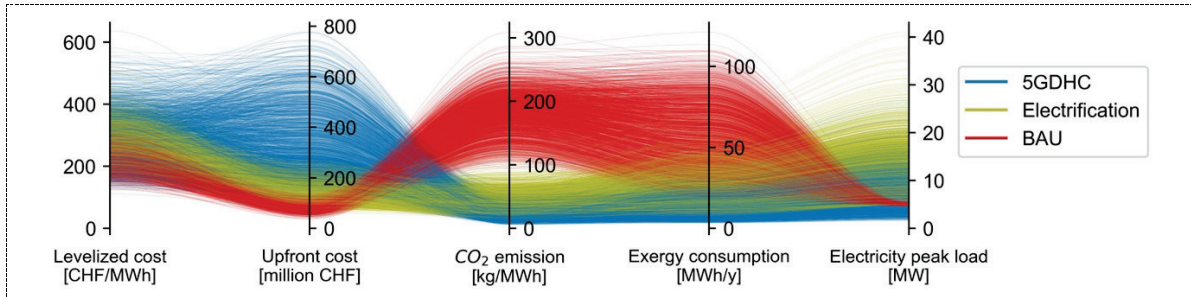


Figure 2. Variation of KPIs of 5GDHC and the reference systems based on the MC runs.

### 2.7.1.3.2 Sources of uncertainty

The results of Sobol analysis for economic indicator ratios between 5GDHC and the Electrification option are presented in Figure 3, showing the three most important parameters. Starting with the comparison of upfront cost, retrofit probability is the most influential parameter, as it is closely related to the total building energy demand and therefore the required capacity of device. It is followed by the price of BHE and ASHP. BHE is the largest contributor to the upfront cost of 5GDHC, while ASHP is the largest contributor in the Electrification option. It is worth mentioning that the scaling factor of pipe cost has insignificant impact on the total investment cost. The influential parameters also have the greatest impact on the levelized cost of energy, as annualized investment cost outweighs fuel and O&M costs in 5GDHC. In addition, discount rate is influential when determining the annuity factor for investment cost. Parameters related to fuel and O&M costs, such as equipment efficiency and O&M cost, have less impact.

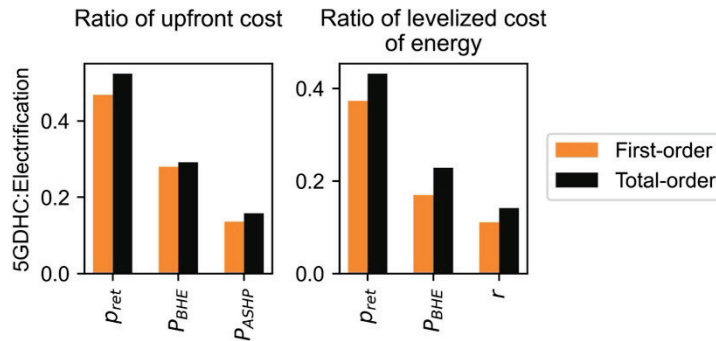


Figure 1. Sobol indices for the ratio of economic indicators between 5GDHC and the Electrification option.

Figure 17 presents the Sobol analysis results of the economic indicator ratios between 5GDHC and the BAU option. The results reveal that retrofit probability and equipment price are the most significant sources of uncertainty when comparing economic performance indicators. In addition, the price of gas also ranks high as the fuel cost holds the largest share of the levelized cost of energy in the BAU option.

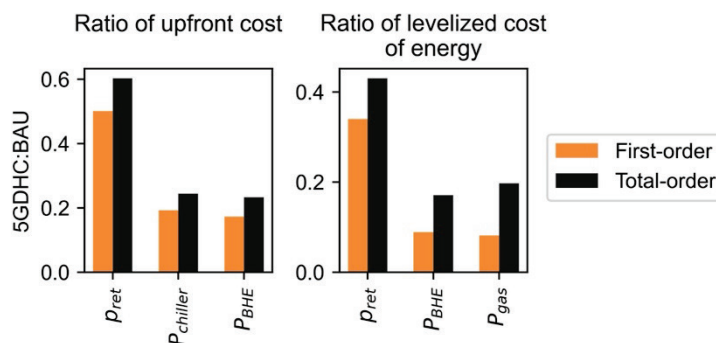


Figure 2. Sobol indices for the ratio of economic indicators between 5GDHC and the BAU option.



### 2.7.1.3.3 Critical parameters driving 5GDHC adoption

Figure 19 and Figure 20 present the critical parameters that determine whether 5GDHC outperform the reference systems economically. These parameters largely coincide with the most influential parameters identified by the Sobol analysis. However, with the results of factor mapping, we can analyse how these parameters affect the relative attractiveness of 5GDHC. When retrofit probability falls in the range of 0.4-0.9, 5GDHC is more likely to outperform the reference systems from a cost perspective. This is because retrofit leads to a ratio of heating and cooling demand that is more favourable to the use of BTES. A lower BHE price also benefits the adoption of 5GDHC. However, a high discount rate is unfavourable for 5GDHC, as it weakens the benefit of reduced fuel cost over time. Furthermore, high gas prices will drive the shift from the BAU option to 5GDHC.

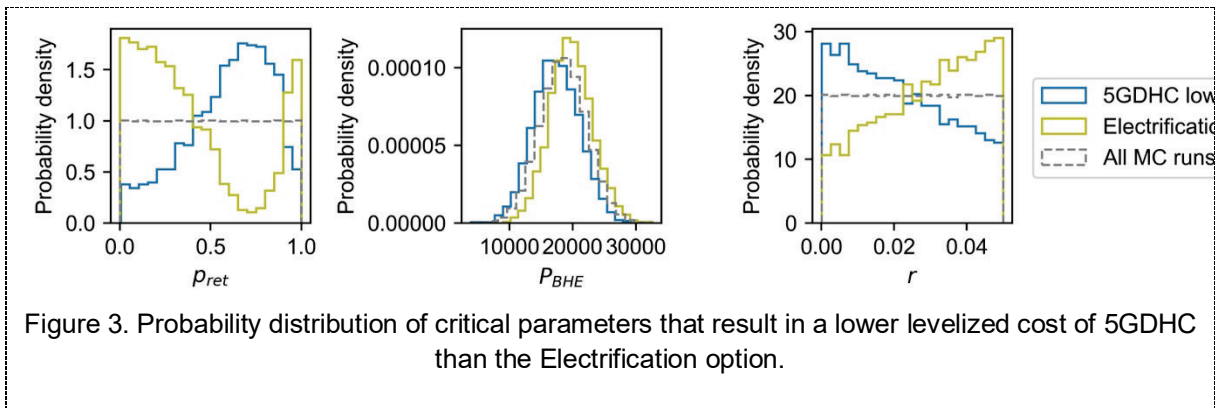


Figure 3. Probability distribution of critical parameters that result in a lower levelized cost of 5GDHC than the Electrification option.

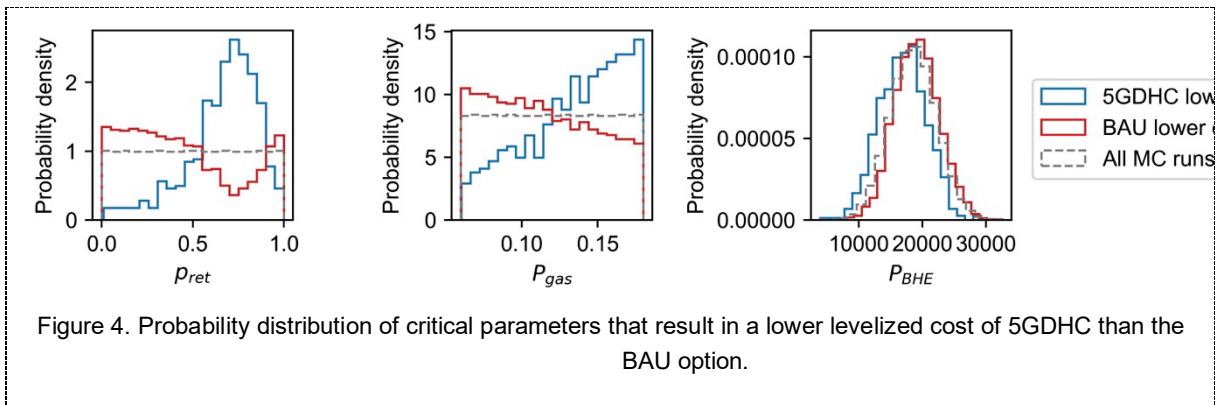


Figure 4. Probability distribution of critical parameters that result in a lower levelized cost of 5GDHC than the BAU option.

The results indicate significant uncertainty in the relative performance of 5GDHC. The attractiveness of 5GDHC is closely linked to the retrofit probability, which affects the magnitude of heating and cooling demands. 5GDHC is a promising technology for combined heating and cooling and could realize potential synergies between them. Gas significantly impacts the economic performance of the BAU option, however its uncertainty is more difficult to address than other sources of uncertainties in 5GDHC, such as equipment price. Adopting 5GDHC has the potential to reduce uncertainty in energy costs. All these aspects indicate growing opportunities for 5GDHC.

## 2.7.2 Hydraulic Modeling of Thermal Grid Systems for Minimizing Pumping Energy Consumption

Aims:

- Perform hydraulic modeling to analyze the thermal grid's performance under various configurations, considering factors such as flow rates, pressure drops, and temperature distribution.
- Optimize pipe and pump sizing to ensure efficient operation and mass balances throughout the thermal grid network, taking into account thermodynamic requirements and hydraulic constraints.



- Quantify the energy consumption of the pump systems to identify the opportunities for energy savings through design optimization.
- Compare and evaluate different hydraulic modeling approaches (i.e., the pressure drop approach and the velocity limit approach) for sizing pipes and pumps within the thermal grid.
- Conduct cost analysis to assess the economic feasibility of different pump options, considering purchase and bare module costs.
- Investigate the system's sensitivity to variations in pipe sizes and the number of buildings connected to the grid, allowing the identification of critical parameters in system design and scalability.

A Monte Carlo Simulation and a Sensitivity Analysis is used to address these questions. The effect of the percentage of the buildings and different pipe sizes are investigated on a double pipe configuration.

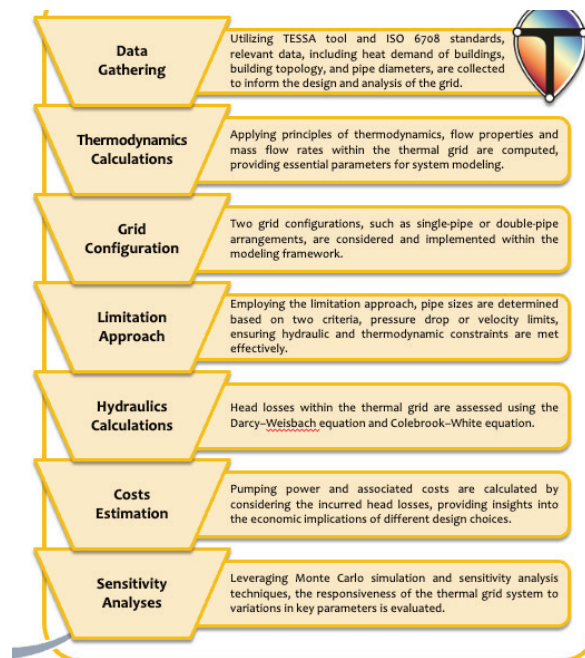


Figure 5. Method overview

Figure 22 shows initial results of this work from a Monte Carlo simulation. These preliminary results indicate that it is better to design a grid for 100% of buildings even if, initially, only a smaller percentage are actually connected. The thermal grid system is less sensitive to variations in the percentage of buildings than to pipe sizes. However, if the proportion of initially connected buildings falls below 90%, constraints related to velocity will arise. As pipe size increases, there is a corresponding decrease in total pumping power consumption. If the grid is initially designed for a lower percentage of buildings and if, eventually, all buildings connect to the grid, total pumping power consumption will be higher compared to a grid that was initially designed for all buildings.

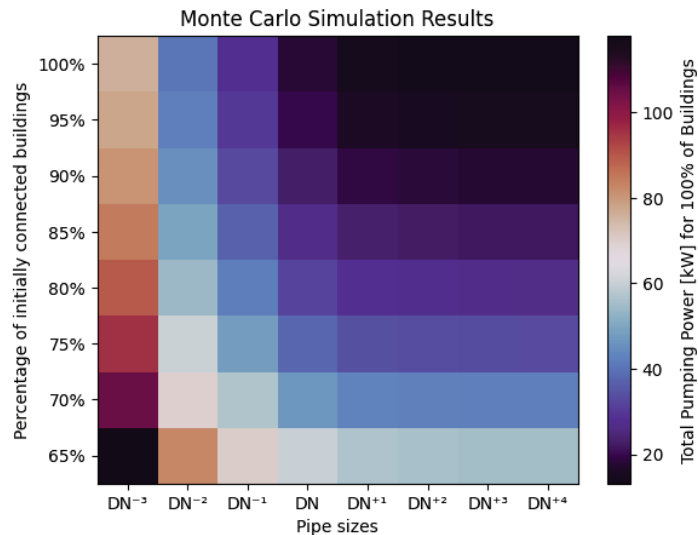


Figure 6. Monte Carlo simulation results of the total pumping power required for a network according to whether the pipes are initially under- or over-sized relative to optimum, as a function of the percentage of initially connected buildings.

### 3 Conclusion

The local thermal system model for district energy decarbonisation is assembled from a number of modules combined. The models used for each module were documented in this deliverable, which complements the code release documented in deliverable report 1.2.1. Methods from previously published works were reproduced in this document in order to provide a more comprehensive collection of model documentation that can be used as a single point of reference for future works and developments. It is anticipated that further expansions of this document will be made to integrate future model works.

### 4 References

- [1] J. Chambers, S. Cozza, and M. Patel, "The GENEAP project: digitalising and automating planning of district heating and cooling," *J. Phys. Conf. Ser.*, vol. 2600, no. 8, p. 082003, Nov. 2023, doi: 10.1088/1742-6596/2600/8/082003.
- [2] S. Schneider, P. Hollmuller, J. Chambers, and M. Patel, "A Heat Demand Load Curve Model of the Swiss National Territory," *IOP Conf. Ser. Earth Environ. Sci.*, vol. 290, no. 1, p. 012107, Jun. 2019, doi: 10.1088/1755-1315/290/1/012107.
- [3] K. N. Streicher, M. Berger, E. Panos, K. Narula, M. C. Soini, and M. K. Patel, "Optimal building retrofit pathways considering stock dynamics and climate change impacts," *Energy Policy*, vol. 152, p. 112220, May 2021, doi: 10.1016/j.enpol.2021.112220.
- [4] J. D. Chambers, "Computationally scalable geospatial network and routing analysis through multi-level spatial clustering," *MethodsX*, p. 101072, Sep. 2020, doi: 10.1016/j.mex.2020.101072.
- [5] CH2018, "CH2018 – Climate Scenarios for Switzerland, Technical Report," 2018.
- [6] Swisstopo, "Karten der Schweiz - Schweizerische Eidgenossenschaft - map.geo.admin.ch." Accessed: Jul. 30, 2019. [Online]. Available: <https://s.geo.admin.ch/82d8014435>
- [7] T. Schluck, K. N. Streicher, and S. Mennel, "Statistical modelling of the energy reference area based on the Swiss building stock," *J. Phys. Conf. Ser.*, vol. 86, no. February, pp. 35–42, Nov. 2019, doi: 10.1002/cjce.20015.
- [8] "Data Packages | Frictionless Data." Accessed: Apr. 30, 2021. [Online]. Available: <https://frictionlessdata.io/data-package/>
- [9] K. N. Streicher, M. Berger, J. Chambers, S. Schneider, and M. K. Patel, "Combined geospatial and techno-economic analysis of deep building envelope retrofit," in *Journal of Physics: Conference Series*, 2019, p. 12028.



- [10] K. N. Streicher, P. Padey, D. Parra, M. C. Bürer, and M. K. Patel, "Assessment of the current thermal performance level of the Swiss residential building stock: Statistical analysis of energy performance certificates," *Energy Build.*, vol. 178, pp. 360–378, Nov. 2018, doi: 10.1016/J.ENBUILD.2018.08.032.
- [11] K. N. Streicher, P. Padey, D. Parra, M. C. Bürer, S. Schneider, and M. K. Patel, "Analysis of space heating demand in the Swiss residential building stock: Element-based bottom-up model of archetype buildings," *Energy Build.*, vol. 184, pp. 300–322, Feb. 2019, doi: 10.1016/J.ENBUILD.2018.12.011.
- [12] K. N. Streicher, S. Mennel, J. Chambers, D. Parra, and M. K. Patel, "Cost-effectiveness of large-scale deep energy retrofit packages for residential buildings under different economic assessment approaches," *Energy Build.*, vol. 215, p. 109870, 2020, doi: <https://doi.org/10.1016/j.enbuild.2020.109870>.
- [13] Swiss Federation, "RegBL | Registre fédéral des bâtiments et des logements." Accessed: Oct. 26, 2020. [Online]. Available: <https://www.housing-stat.ch/fr/accueil.html>
- [14] S. Cozza, M. K. Patel, and J. Chambers, "Uncertainty in potential savings from improving energy label: A Monte Carlo study of the Swiss residential buildings," *Energy Build.*, vol. 271, p. 112333, Sep. 2022, doi: 10.1016/j.enbuild.2022.112333.
- [15] F. Sasso and M. K. Patel, "Thermal performance of residential and non-residential sectors: describing differences and understanding underlying reasons," *J. Phys. Conf. Ser.*, vol. 2600, no. 2, p. 022003, Nov. 2023, doi: 10.1088/1742-6596/2600/2/022003.
- [16] S. Schneider, P. Hollmüller, P. Le Strat, J. Khoury, M. Patel, and B. Lachal, "Spatial–Temporal Analysis of the Heat and Electricity Demand of the Swiss Building Stock," *Front. Built Environ.*, vol. 3, p. 53, Aug. 2017, doi: 10.3389/fbuil.2017.00053.
- [17] "JASM - Home Page." Accessed: Jun. 12, 2020. [Online]. Available: <https://sccer-jasm.ch/>
- [18] X. Li, J. Chambers, S. Yilmaz, and M. K. Patel, "A Monte Carlo building stock model of space cooling demand in the Swiss service sector under climate change," *Energy Build.*, vol. 233, p. 110662, Feb. 2021, doi: 10.1016/j.enbuild.2020.110662.
- [19] X. Li, J. Chambers, S. Yilmaz, and M. K. Patel, "A Monte Carlo building stock model of space cooling demand in the Swiss service sector under climate change," *Energy Build.*, vol. 233, p. 110662, Feb. 2021, doi: 10.1016/j.enbuild.2020.110662.
- [20] J. D. Chambers *et al.*, "Evaluating the electricity saving potential of electrochromic glazing for cooling and lighting at the scale of the Swiss non-residential national building stock using a Monte Carlo model," *Energy*, vol. 185, pp. 136–147, Oct. 2019, doi: 10.1016/J.ENERGY.2019.07.037.
- [21] J. Chambers and A. James, "PACE REFIT building archetype load curves." Université de Genève, Yareta, 2022. doi: 10.26037/YARETA:TCTXN4DCTVDAJOK4VLUFLECGSA.
- [22] J. Chambers *et al.*, "Evaluating the electricity saving potential of electrochromic glazing for cooling and lighting at the scale of the non-residential national building stock using a Monte Carlo model," *Energy*, vol. 185, pp. 136–147, 2019, doi: 10.1016/j.energy.2019.07.037.
- [23] D. C. Montgomery, E. A. Peck, G. G. Vining, and G. G. Vining, "Introduction to linear regression analysis," no. 2012, 2012, pp. 171–210.
- [24] CH2018, "CH2018 – Climate Scenarios for Switzerland, Technical Report," 2018.
- [25] D. N. Bird, R. de Wit, H. P. Schwaiger, K. Andre, M. Beermann, and M. Žuvela-Aloise, "Estimating the daily peak and annual total electricity demand for cooling in Vienna, Austria by 2050," *Urban Clim.*, vol. 28, p. 100452, 2019, doi: 10.1016/j.uclim.2019.100452.
- [26] M. Isaac and D. P. van Vuuren, "Modeling global residential sector energy demand for heating and air conditioning in the context of climate change," *Energy Policy*, vol. 37, pp. 507–521, 2009, doi: 10.1016/j.enpol.2008.09.051.
- [27] M. Jakubcionis and J. Carlsson, "Estimation of European Union service sector space cooling potential," *Energy Policy*, vol. 113, pp. 223–231, 2017, doi: 10.1016/j.enpol.2017.11.012.
- [28] H. Asloune *et al.*, "Prospective Modelling of Residential Space Cooling Diffusion in France," 2019.
- [29] S. van der Walt, S. C. Colbert, and G. Varoquaux, "The NumPy Array: A Structure for Efficient Numerical Computation," *Comput. Sci. Eng.*, vol. 13, no. 2, pp. 22–30, Mar. 2011, doi: 10.1109/MCSE.2011.37.
- [30] E. Jones, T. Oliphant, P. Peterson, and others, "SciPy: Open source scientific tools for Python." 2015.
- [31] W. McKinney, "pandas: a Foundational Python Library for Data Analysis and Statistics".
- [32] S. Hoyer and J. Hamman, "xarray: N-D labeled arrays and datasets in Python," *Prep J Open Res Softw.*, 2016.



- [33] S. K. Lam, A. Pitrou, and S. Seibert, "Numba: a LLVM-based Python JIT compiler," in *Proceedings of the Second Workshop on the LLVM Compiler Infrastructure in HPC*, H. Finkel, Ed., Austin, Texas, USA: ACM, 2015. doi: 10.1145/2833157.
- [34] J. D. Hunter, "Matplotlib: A 2D Graphics Environment," *Comput. Sci. Eng.*, vol. 9, no. 3, pp. 90–95, 2007, doi: 10.1109/MCSE.2007.55.
- [35] Met Office, "Cartopy: a cartographic python library with a matplotlib interface." Exeter, Devon, 2016.
- [36] Federal Office of Topography, "swisstopo Homepage." Accessed: Jan. 29, 2018. [Online]. Available: <https://www.swisstopo.admin.ch/>
- [37] S. Schneider, P. Hollmuller, J. Chambers, and M. Patel, "A Heat Demand Load Curve Model of the Swiss National Territory," *IOP Conf. Ser. Earth Environ. Sci.*, vol. 290, no. 1, p. 12107, 2019, doi: 10.1088/1755-1315/290/1/012107.
- [38] J. Chambers, K. Narula, M. Sulzer, and M. K. Patel, "Mapping district heating potential under evolving thermal demand scenarios and technologies: A case study for Switzerland," *Energy*, vol. 176, pp. 682–692, Jun. 2019, doi: 10.1016/J.ENERGY.2019.04.044.
- [39] J. Chambers *et al.*, "Spatiotemporal analysis of industrial excess heat supply for district heat networks in Switzerland," *Energy*, vol. 192, p. 116705, Feb. 2019, doi: 10.1016/j.energy.2019.116705.
- [40] M. Ester, H.-P. Kriegel, J. Sander, and X. Xu, "A Density-Based Algorithm for Discovering Clusters," *Proc. Second Int. Conf. Knowl. Discov. Data Min.*, 1996, doi: 10.1016/B978-044452701-1.00067-3.
- [41] C. Malzer and M. Baum, "A Hybrid Approach To Hierarchical Density-based Cluster Selection," Nov. 2019, Accessed: Mar. 19, 2020. [Online]. Available: <http://arxiv.org/abs/1911.02282>
- [42] X. Li, A. Walch, S. Yilmaz, M. Patel, and J. Chambers, "Optimal spatial resource allocation in networks: Application to district heating and cooling," *Comput. Ind. Eng.*, vol. 171, p. 108448, Sep. 2022, doi: 10.1016/j.cie.2022.108448.
- [43] A. Walch *et al.*, "Shallow geothermal energy potential for heating and cooling of buildings with regeneration under climate change scenarios," Dec. 2021, Accessed: Dec. 13, 2021. [Online]. Available: <http://arxiv.org/abs/2112.01183>
- [44] J. Chambers, "Computationally scalable geospatial network and routing analysis through multi-level spatial clustering.," *MethodsX*, vol. 7, no. June, p. 101072, 2020, doi: 10.1016/j.mex.2020.101072.
- [45] X. Li, S. Yilmaz, M. K. Patel, and J. Chambers, "Techno-economic analysis of fifth-generation district heating and cooling combined with seasonal borehole thermal energy storage," *Energy*, vol. 285, p. 129382, Dec. 2023, doi: 10.1016/j.energy.2023.129382.
- [46] M. Cimmino, "A finite line source simulation model for geothermal systems with series- and parallel-connected boreholes and independent fluid loops," *J. Build. Perform. Simul.*, vol. 11, no. 4, pp. 414–432, Jul. 2018, doi: 10.1080/19401493.2017.1381993.
- [47] A. Zarrella, G. Emmi, and M. De Carli, "A simulation-based analysis of variable flow pumping in ground source heat pump systems with different types of borehole heat exchangers: A case study," *Energy Convers. Manag.*, vol. 131, pp. 135–150, Jan. 2017, doi: 10.1016/j.enconman.2016.10.061.
- [48] J. Chambers, M. J. S. Zuberi, K. N. Streicher, and M. K. Patel, "Geospatial global sensitivity analysis of a heat energy service decarbonisation model of the building stock," *Appl. Energy*, vol. 302, p. 117592, 2021, doi: 10.1016/j.apenergy.2021.117592.
- [49] X. Li, J. Chambers, S. Yilmaz, and M. Patel, "Sensitivity analysis of fifth generation district heating and cooling coupled with borehole thermal energy storage," presented at the CISBAT, 2023.
- [50] G. Mavromatidis, K. Orehounig, and J. Carmeliet, "Uncertainty and global sensitivity analysis for the optimal design of distributed energy systems," *Appl. Energy*, vol. 214, pp. 219–238, Mar. 2018, doi: 10.1016/j.apenergy.2018.01.062.
- [51] A. Saltelli *et al.*, *Global sensitivity analysis: the primer*. John Wiley & Sons, 2008.
- [52] A. Saltelli, Ed., *Sensitivity analysis in practice: a guide to assessing scientific models*. Hoboken, NJ: Wiley, 2004.
- [53] F. J. Massey Jr, "The Kolmogorov-Smirnov test for goodness of fit," *J. Am. Stat. Assoc.*, vol. 46, no. 253, pp. 68–78, 1951.